ELSEVIER

Contents lists available at ScienceDirect

Materials Science & Engineering C

journal homepage: www.elsevier.com/locate/msec



Infection-prevention on Ti implants by controlled drug release from folic acid/ZnO quantum dots sealed titania nanotubes



Yiming Xiang^a, Xinmei Liu^b, Congyang Mao^a, Xiangmei Liu^a, Zhenduo Cui^c, Xianjin Yang^c, Kelvin W.K. Yeung^d, Yufeng Zheng^e, Shuilin Wu^{a,c,*}

- ^a Hubei Collaborative Innovation Center for Advanced Organic Chemical Materials, Ministry-of-Education Key Laboratory for the Green Preparation and Application of Functional Materials, Hubei Key Laboratory of Polymer Materials, School of Materials Science & Engineering, Hubei University, Wuhan 430062, China
- ^b Northwest Institute for Non-ferrous Metal Research, Xi an 710016, China
- ^c School of Materials Science & Engineering, Tianjin University, Tianjin 300072, China
- d Department of Orthopaedics & Traumatology, Li Ka Shing Faculty of Medicine, The University of Hong Kong, Pokfulam, Hong Kong, China
- ^e China State Key Laboratory for Turbulence and Complex System, Department of Materials Science and Engineering, College of Engineering, Peking University, Beijing 100871. China

ARTICLE INFO

Keywords: ZnO Quantum dots Drug delivery pH sensitivity Antibacterial Infection prevention

ABSTRACT

Bacterial infections and related complications are predominantly responsible for the failure of artificial biomaterials assisted tissue regeneration in clinic. In this work, a hybrid surface system is applied to prolong the drug release duration from dug-loaded titania nanotubes and thus to prevent Ti implants-associated bacterial infections. This feature is endowed by conjugating folic acid (FA) onto the surface of ZnO quantum dots (QDs)-NH $_2$ via an amidation reaction. Titania nanotubes (TNTs) loaded with vancomycin (Van) are capped by these FA functionalized ZnO (ZnO-FA) QDs that keep stable in normal physiological environments but dissolves to Zn 2 in the mildly acidic environment after bacterial infections as validated by the drug release profile. The antibacterial ratio of TNTs-Van@ZnO-FA QDs against Staphylococcus aureus is enhanced from 60.8% to 98.8%while this value is only increased from 85.2% to 95.1% for TNTs-Van once the pH value of the environment is decreased from 7.4 to 5.5. This is due to the synergistic effects of Van and Zn 2 because the gradual dissolution of ZnO-FA caps on TNTs with the decrease of pH value can induce the acceleration of both Van and Zn 2 release. In addition, this TNTs-Van@ZnO-FA system also exhibits excellent biocompatibility because of the folic acid and sustained release of Zn ions. Hence, this surface system can be potentially used as a promising bioplatform on Ti-based metallic implants to prevent bacterial infection with a long-lasting effect.

1. Introduction

Since 1950s, Ti-based alloys have been commonly applied as orthopaedic implant materials for hard tissue repair or reconstruction because of their desirable mechanical strength, corrosion resistance, and biocompatibility [1–4]. However, implant failure arising from post-surgery infection is one of the most serious complications after surgery [5]. Antibacterial biomaterials exhibit the greatest potential to prevent bacterial infections [6–8]. Clinically, antibiotics treatment is usually prescribed to prevent infection-related complications, but systemic drug administration, regardless of whether it is intravenous, intramuscular, or topical, exhibits some shortcomings such as low drug solubility, uncontrolled pharmacokinetics, and serious side-effects on non-target tissues. Therefore, local antibiotics delivery to the sites of

implantation is preferred, which is commonly conducted via antibiotics-loaded bone cement clinically [9,10]. Vancomycin (Van), penicillin, and antimicrobial peptides have been applied for this purpose because they can mitigate inflammation and inhibit bacteria growth [11,12]. Owing to their excellent biocompatibility, large specific surface area and tubular structure, titania nanotubes (TNTs) have attracted much attention of biomaterials scientists and orthopaedic surgeons because these characteristics can favor the loading of drugs or antibacterial agents [13,14]. In addition, uniform TNTs arrays can be easily produced on the surface of Ti-based alloys [15–17].

However, the loaded drugs in pure TNTs alone can result in a rapid release [18–20], which leads to the overdose within a short time at local area and is not beneficial for long-lasting prevention of bacterial infections. Therefore, the ideal drug-loading system on implants should

^{*} Corresponding author at: Hubei Collaborative Innovation Center for Advanced Organic Chemical Materials, Ministry-of-Education Key Laboratory for the Green Preparation and Application of Functional Materials, Hubei Key Laboratory of Polymer Materials, School of Materials Science & Engineering, Hubei University, Wuhan 430062, China.

E-mail address: shuilinwu@tju.edu.cn (S. Wu).

meet the practical requirements, i.e., the system can tune the drug release behaviors according to the degree of infections. Great efforts have been made to cover TNTs loaded with drugs to improve the drug release behaviors [14,17,21,22].

Considering the local acidification induced by bacterial infections, ZnO nanostructures can be applied for the encapsulation of drugs due to their gradual dissolution in acidic environments [23,24]. In addition, zinc is a necessary trace element in human body, which plays a significant role in human and cell development [25,26]. Recent studies report that zinc ions have good antibacterial properties [27,28], but excessive zinc ions can lead to cytotoxicity [29,30]. ZnO QDs are sensitive to pH change, i.e., they are stable at normal physiological pH but dissolved in acid environments [31,32]. The amount of zinc ions in the dissolving process is not too much to cause cytotoxicity. In addition, ZnO QDs are inexpensive and can be prepared easily. These superiorities make ZnO QD a satisfactory candidate as a gatekeeper to fabricate pH-responsive drug-loading system for enhancing the surface antibacterial ability [33–36].

Nevertheless, the unmodified ZnO QDs cannot cover the TNTs directly and are easily swallowed by cells [37,38]. Thus they are not conducive to the growth of osteoblasts. Folic acid (FA) plays a significant role for human to make DNA, RNA, and amino acids that are required for cell division [39–41]. Furthermore, FA has many chemical groups that can form metal complex with metal particles [35,42]. Therefore, in this work, we have developed a pH sensitive surface gatekeeper system on TNTs, in which ZnO QDs are chemically coordinated by FA and subsequently grafted onto TNTs. The fabrication process and related release mechanism are schematically illustrated in Scheme 1.

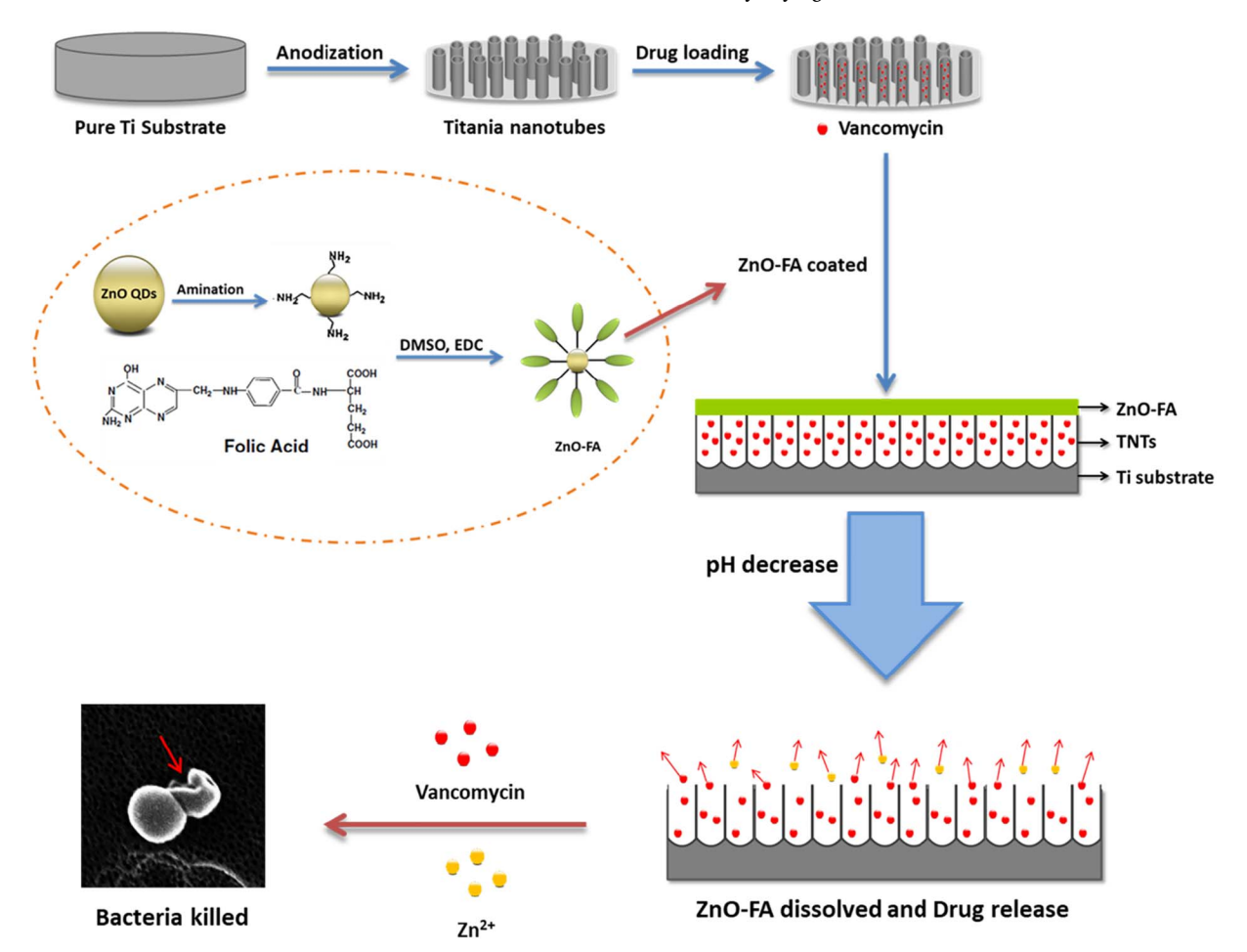
2. Materials and method

2.1. Preparation of Ti samples

Pure titanium plates ($\delta=2$ mm, $\phi=6$ mm) were first mechanically polished with SiC sandpaper of various grades then cleaned with deionized water and ethanol using an ultrasonic cleaner. The over-dried samples were chemically etched in mixed solution of HF, HNO3 and H2O with volume ratio of 1:4:5. The TNT arrays were synthesized on a two-electrode DC anodization system in the electrolyte contained ethylene glycol, NH4F, and H2O at 60 °C for 1 h. The anodization voltage was 30 V and fluoride concentration was 0.03 M [16,17]. Then, the obtained TNTs were annealed at 450 °C for 2 h and subsequently washed with ethyl alcohol and deionized (DI) water. Finally, these TNTs samples were dried in a vacuum oven for further use.

2.2. Synthesis of ZnO QDs

Zinc acetate (440 mg, 2.0 mmol) and magnesium acetate (44 mg, 0.2 mmol) were dissolved in hot ethanol (30 mL) under vigorous stirring. In a separate flask, NaOH (100 mg, 2.5 mmol) was dissolved in refluxing ethanol (10 mL). The solutions were then cooled down in an ice bath. Subsequently, the NaOH solution was then rapidly injected into the flask containing zinc acetate and magnesium acetate. The mixture was stirred for 8 h for particle growth, and the resulting transparent quantum dots 02 dispersion showed green emission under UV lamp excitation (365 nm). Finally, these ZnO QDs were precipitated using hexane as a nonsolvent and washed with ethanol three times followed by drying in a vacuum oven.



Scheme 1. The schematic illustration of fabrication process of TNTs-Van@ZnO-FA system and synergistic bacteria-killing triggered by pH.

2.3. Synthesis of amine-grafted ZnO QDs

ZnO QDs (100 mg) were dispersed ultrasonically in anhydrous N, N'-dimethylformamide (DMF, 15 mL). After adding 3-Aminopropyltriethoxysilane (APTES, 50 μ L), the solution was stirred at 120 °C for 15 min and followed by centrifugation, then washed with DMF to collect the amine-functionalized ZnO (ZnO-NH₂) QDs.

2.4. Synthesis of ZnO QDs-conjugated FA coating

The FA modified ZnO QDs were carried out by following process. Briefly, FA (1.0 mg) was dissolved in 0.5 mL of dimethyl sulfoxide (DMSO), then 1.0 mg 1-(3-dimethylaminopropyl)-3-ethylcarbodiimide hydrochloride (EDC) was added into the above FA solution and stirred for 30 min to obtain activated FA solution. Next, the as-prepared activated solution was added into 10.0 mL of 1 mg mL $^{-1}$ ZnO-NH $_2$ QDs aqueous solution with continuous stirring for 6 h at room temperature.

2.5. Drug loading and release study

A solution of vancomycin (Van) (10 mg/mL) was prepared in DI water as the model drug. The as-prepared TNTs samples were immersed into Van solution, for 2 days to load drugs and followed by drying in air. The samples were named TNTs-Van.

 $100~\mu L$ ZnO-FA solution of 1 mg/mL was coated onto the surface of TNTs-Van samples by spin-coating method. The process was conducted on the spin coater (KW-4A) at room temperature with given times. These samples were named TNTs-Van@ZnO-FA. Drug release from the both TNTs-Van and TNTs-Van@ZnO-FA was investigated by immersion specimens (n = 5) were immersed in 100 mL of phosphate buffered saline (PBS) at 37 °C, and the amount of released drugs was determined by ultraviolet–visible (UV–vis) spectrophotometry.

The measurements were taken at short intervals during the first 5 h to monitor the initial burst release, followed by testing every 24 h to observe the long-term release behaviors until all the drugs had been released to the PBS. The samples were immersed in 10 mL of PBS (pH 7.4, 6.4, 5.4 and 4.5) in the absence of light. At setting time, 10 mL PBS were taken out for testing and refreshed by the same volume fresh PBS. The absorbance at 280 nm was recorded and the corresponding Van concentration was determined from the calibration curve of Van in PBS. The percentage of drug release was calculated by dividing the accumulated amount of released drugs by the total loaded amount. The total amount of loading drugs was the released drugs at the end of the experiment when the UV–vis absorption spectra did not change any more. For each time interval, the samples were tested and the means and standard deviations were used in the data analysis.

2.6. Characterization

The morphology and composition of the modified surface were investigated by field emission scanning electron microscopy (FE-SEM, JSM7100F) and scanning electron microscopy (SEM, JEOL-820 and JSM6510LV) equipped with energy-dispersive spectroscopy (EDS). X-ray diffraction (XRD, Rigaku, D/Max-RB), X-ray photoelectron spectroscopy (XPS, Thermo Fisher Scientific 250Xi), Fourier transform infrared spectroscopy (FTIR, NICOLEF 5700), Transmission electron microscope (TEM; Tecnai G20, FEI, USA) and selected area electron diffraction were employed to determine the microstructures of ZnO QDs.

2.7. Antibacterial tests

Van was only effective against Gram-positive bacteria, especially sensitive to *Staphylococcus aureus* (*S. aureus*). So *S. aureus* was used to evaluate the antibacterial activity of the composite coatings using agarplating method and cultured with a Luria-Betani (LB) culture medium.

To test the antibacterial ratio of the samples, different samples were placed into a 96-well plate, and 200 μL diluted bacterial suspension (10 7 CFU/mL) was incubated with LB culture medium (pH 7.4, 6.4, 5.4 and 4.5) in each well. Then, the well plate was cultured in an incubator at 37 °C for 24 h. Three parallel samples in each group were used for the antibacterial test, and the untreated Ti samples were served as the control group. After that, 20 μL diluted bacterial solution were then coated on the culture dish covered with LB agar, and the samples were incubated at 37 °C for 24 h. The bacterial colony on the plates was observed by a digital camera, and the number of colonies was counted. The antibacterial efficacy was calculated as follows:

 $\mbox{Antibacterial ratio (\%)} = \frac{-\mbox{ number of CFUs in experimental group)}}{\mbox{number of CFUs in control group}} \\ \times 100\%$

The morphology of S. aureus was observed by SEM. For SEM examination, these samples were put into 96-well plates with bacteria suspension. After incubation at 37 °C for 8 h, the bacterial suspension was removed; the bacteria were fixed with a 2.5% glutaraldehyde solution for 2 h, and then dehydrated in gradient ethanol solution of 30%, 50%, 70%, 90% and 100% for 15 min sequentially. Those samples were dried at room temperature for SEM.

2.8. Cell culture

Mouse calvarial cells (MC3T3-E1) were cultured in α -MEM (HyClone) containing 10% fetal bovine serum (FBS) and 1% penicillinstreptomycin solution (HyClone) in a humidified atmosphere of 5% CO2 at 37 °C, with the medium changed every three days. The culturing process has been reported in our previously work [43].

2.9. Cytotoxicity evaluation

The cytotoxicity level for cell cultures on samples was assessed using a 3-[4, 5-dimethylthiazol-2-yl]-2, 5-diphenyl tetrazolium bromide (MTT) assay. Before the MTT assay, pure Ti samples were served as the control, and all specimens were incubated in 96-well plates with the MC3T3 cell was seeded in it. After culturing for 1, 3 and 7 days, 200 MTT μL solutions with a concentration of 5 $\mu g/mL$ was added to each well and incubated for 4 h at 37 °C. Then the medium was removed, and 200 μL of DMSO was added to the well, followed by the incubation of a color reaction for 15 min at a shaking table. After that, the supernatant fluid was fetched out to test the optical density with SpectraMax i3 Platform (Molecular Devices, California, USA) at a wavelength of 490 nm. The detail procedure can be found in our previous publication [44]. All measurements were taken in triplicate.

In addition, at 1 day, the cell fluorescence was detected by cell staining. At 1 day the cells were washed thrice with PBS (pH = 7.4) and fixed in 4% formaldehyde solution for 10 min at room temperature, and rinsed thoroughly with PBS. Then, the samples were stained with FITC-Phalloidin (YiSen, Shanghai) at room temperature in darkness for 30 min and further stained with 40,6-diamidino-2-phenylindole dihydrochloride (DAPI) (YiSen, Shanghai) for 30 min in darkness. The cell morphology on different samples was examined by fluorescence microscope (IFM, Olympus, IX73). The morphologies of cells on samples were observed by SEM, and the cell fixation process was the same as bacteria fixation.

3. Results and discussion

3.1. Characterization of TNTs and QDs

Fig. 1A depicts the FE-SEM images of the TNTs prepared on Ti substrate. The TNTs are orderly and uniform with an inner diameter of

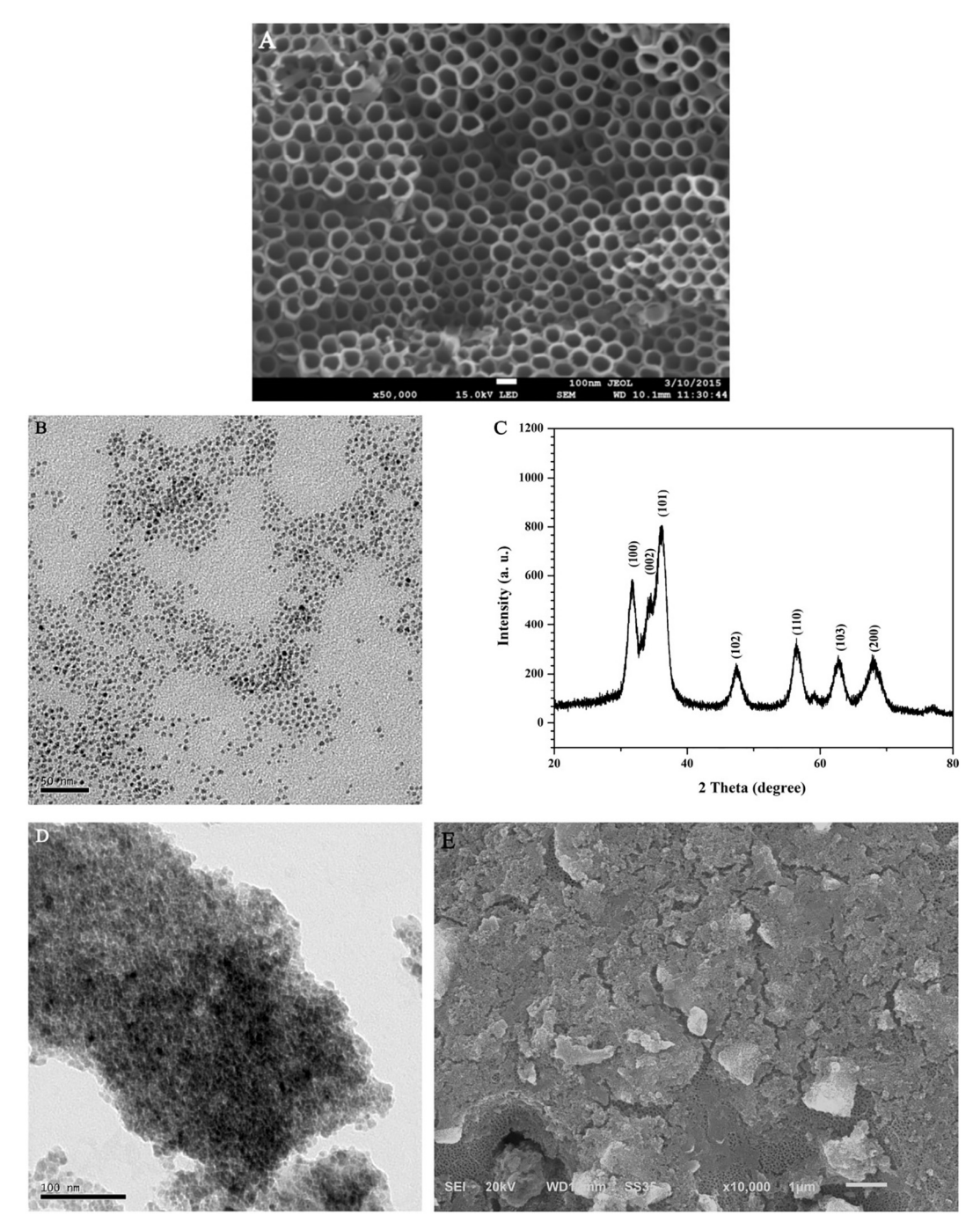


Fig. 1. (A) Morphological and microstructural characterization of FE-SEM image of TNTs. (B) TEM images of ZnO QDs, (C) XRD patterns of ZnO QDs. (D) TEM images of ZnO-FA. (E) SEM image of TNTs-Van@ZnO-FA.

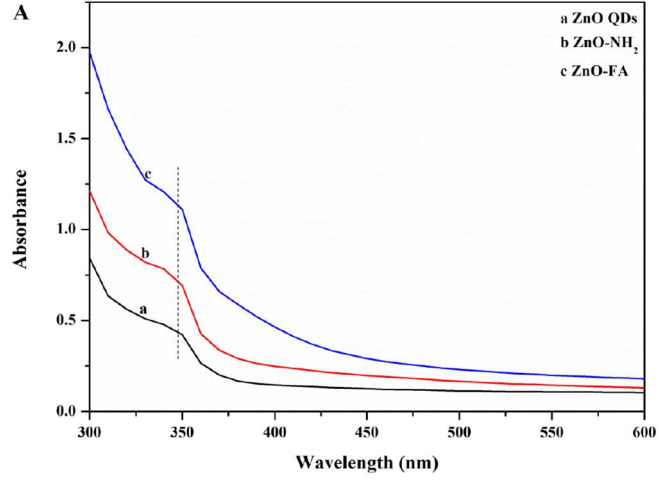
about 80 nm. A TEM micrograph of the chemically synthesized ZnO QDs is presented in Fig. 1B. The TEM micrograph suggests near monodisperse ZnO QDs with an average size of 3–5 nm. The corresponding selected area electron diffraction (SAED) pattern is shown in Fig. S1, exhibits the highly polycrystalline nature of the as-prepared ZnO QDs. To further confirm the phase structure of the prepared ZnO, these ZnO QDs were examined by XRD. In Fig. 1C, the diffraction peaks are located at $2\theta = 31.88^{\circ}$, 34.41° , 36.26° , 47.52° and 56.62° , and all of the diffraction peaks can be clearly indexed to the wurtzite crystal structure with lattice constant a = 0.325 nm and c = 0.521 nm, which are attributed to the typical wurtzite structure of ZnO (JCPDS file no. 36-1451) [45–47].

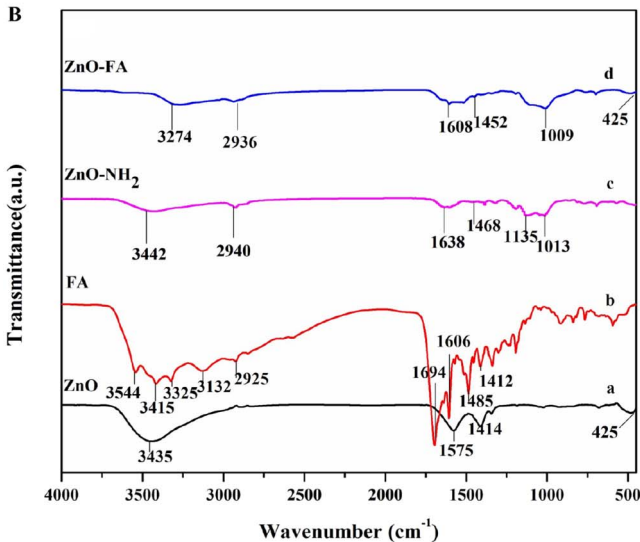
As shown in Fig. 1D, TEM image discloses that FA modified ZnO

QDs are mostly bounded together through FA, which is suitable for capping TNTs as a gatekeeper, and corresponding high magnification TEM image is shown in Fig. S2. In Fig. 1E, the entire surface of TNTs is completely covered by ZnO-FA.

3.2. Phase and morphology examination of the ZnO QDs conjugates

Fig. 2A shows a UV–vis absorbance spectra change of ZnO QDs. ZnO QDs, ZnO-NH $_2$ and ZnO-FA- exhibit the same absorbance at 340 nm (curve a, b and c). There are no significant differences in the absorption features. Fig. 2B shows the FTIR spectra of the prepared QDs. For the assynthesized QDs, the characteristic absorption bands mainly originate from the ZnO QDs. As for curve a, the vibration at 425 cm $^{-1}$ is





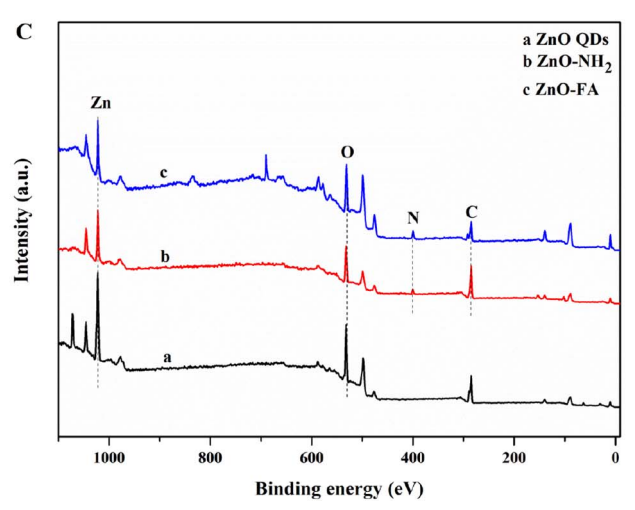


Fig. 2. Characterization of ZnO-FA Conjugates: (A) UV–vis absorbance spectra of (a) ZnO QDs, (b) ZnO-NH₂, (c) ZnO-FA. (B) FTIR spectra of (a) ZnO QDs, (b) FA, (c) ZnO-NH₂, (d) ZnO-FA. (C) XPS of (a) ZnO QDs, (b) ZnO-NH₂, (c) ZnO-FA.

attributed to the Zn–O bond from the ZnO QDs. The FTIR spectrum of the FA is presented in curve b, which is characterized by the bands between 3000 and 3600 cm $^{-1}$ that are attributed to the vibration adsorption of hydroxyl and primary amino group at 3415 and 3325 cm $^{-1}$, the antisymmetric and symmetric stretching vibration of -N-H in $-NH_2$ groups at 3544 cm $^{-1}$, and the vibration adsorption of -O-H in

—OOH groups [39]. The adsorption peaks of 1638 cm⁻¹ and 1606 cm⁻¹ belong to the vibration adsorption of the C=O bond of a −CONH₂ group and the -NH group. The peak at 1485 cm⁻¹ relates to the benzene ring belongs to FA [48]. For comparison, FTIR spectra of ZnO-NH₂ and ZnO-FA are shown in curve c and curve d. In curve c, the bonding of APTES to the surface ZnO QDs was established by the presence of bands at 1135 and 1013 cm⁻¹ which were assigned to Si−O groups, and the two bands at 3442 and 1638 cm⁻¹ are attributed to the N−H stretching vibration and NH₂ bending mode of the free NH₂ groups, respectively [32,35]. These characteristics have proven that ZnO QDs has been successfully functionalized by amino. In curve d, the disappearance of two peaks of NH₂ at 3442 and 1638 cm⁻¹ could prove the conjugation of FA onto the surface of ZnO QDs. The typical FA band located at 1608 cm⁻¹ and 425 cm⁻¹ peak of Zn−O bond further imply the successful conjugation [49].

In Fig. 2C, the peaks located at 1021.3, 531.1 and 284.6 eV were attributed to Zn 2p, O 1s and C 1s, respectively. The new peaks at 399.3 eV in both ZnO-NH2 and ZnO-FA are attributed to N 1s, further confirming the conjugation of NH2 and FA highly in accordance with the FTIR result [50,51]. The high-resolution spectra of Zn 2p, O 1s and C 1s are shown in Fig. S3. Obviously, the binding energy of Zn $2p_{3/2}$ and Zn $2p_{1/2}$ is 1024.1 and 1046.7, respectively, in accordance with our previous study [46]. After the addition of FA, the intensity of Zn2p peak is decreased (comparing Fig. S3A to Fig. S3B) and O1s peak is increased (comparing Fig. S3C to Fig. S3D), because the ZnO was covered by FA [50]. In addition, the O1s spectrum in Fig. S3D is wider than in Fig. S3C due to the introduction of O-C from FA and the fitting curve displays three peaks in Fig. S3D, i.e., peaks at 530.4 and 531.8 eV correspond to O-Zn from ZnO and O-C from FA, respectively, while the peak at 531 eV could be due to the contamination. As shown in Fig. S3E, the C1s peaks of ZnO show binding energy at 285.5 and 288.5 eV, which are possibly originated from surface contamination (CO₂ and organics in air). In Fig. S3F, the high-resolution scan for C1s from ZnO-FA shows a broad shoulder between 281 and 290 eV, and in the fitting curve, the peaks at 284.6, 286.4 and 288.2 eV are attributed to -C-C- bond, -NHCO-bond and -COOH bond, respectively, while the peak at 285.6 is attributed to the contamination. These signals originated from the functional groups of FA [52,53]. All of these results confirmed that FA was successfully grafted onto the surface of ZnO QDs.

3.3. The effect of pH on ZnO QDs capping

The dissolution behavior of the as-prepared ZnO QDs was demonstrated in buffers with different pH (7.4, 5.5), followed by photographing the QDs and detecting the fluorescence spectra. Fig. 3A showed the color changes of ZnO QDs conjugates when exposed to the white light and UV irradiation under neutral and acidic conditions. Under neutral condition, all samples fluoresce when exposed to UV light while they show no fluorescence under white light, proving that ZnO QDs were successfully synthesized. In contrast, the fluorescence of ZnO QDs conjugates were rapidly quenched when the pH of the buffer was reduced to 5.5 due to the acid dissolution of ZnO ODs. These results confirmed the efficiently dissolution of ZnO QDs in an acidic environment. As shown in Fig. 3B, the emission peak of pristine ZnO QDs is located at 527 nm under neutral condition while no emission peak appears under an acidic environment with an excitation of 340 nm, indicating the acidic dissolution of pristine ZnO QDs. In Fig. 3C, with the excitation of 340 nm, amino functionalized ZnO QDs also shows emission peak at 557 nm and the emission peak disappears under an acidic environment, which could prove that the amination process of pristine ZnO QDs makes no difference on its fluorescence effect and just causes a slight redshift [50]. In Fig. 3D, emission peaks at 475 nm can be observed at neutral condition while the emission peaks of ZnO-FA disappear under acidic environment, substantiating the pH-sensitive decomposition of the ZnO-FA. In addition, there exists a peak at 475 nm in Fig. 3D (curve b), indicating the FA has a little bit protective effect on

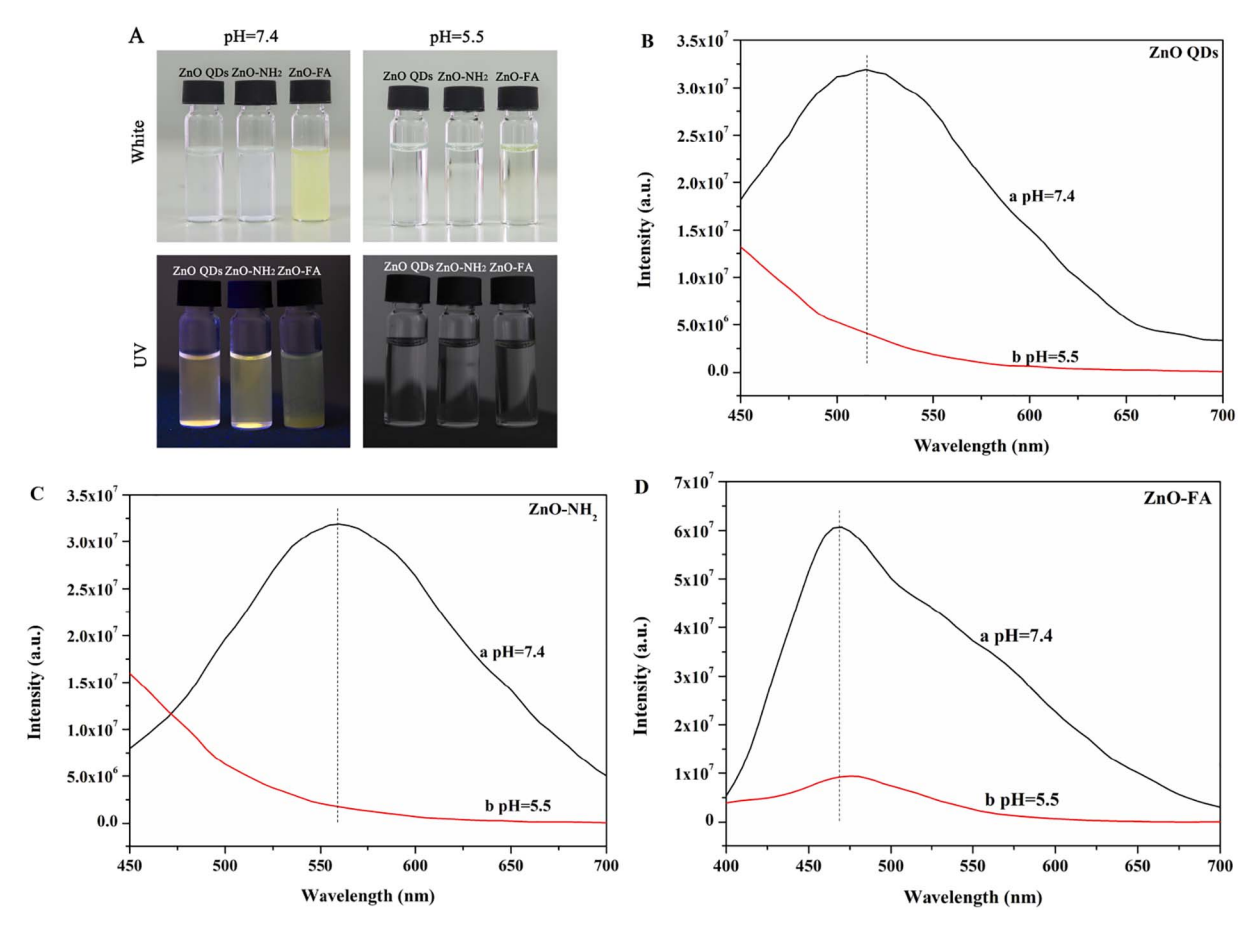


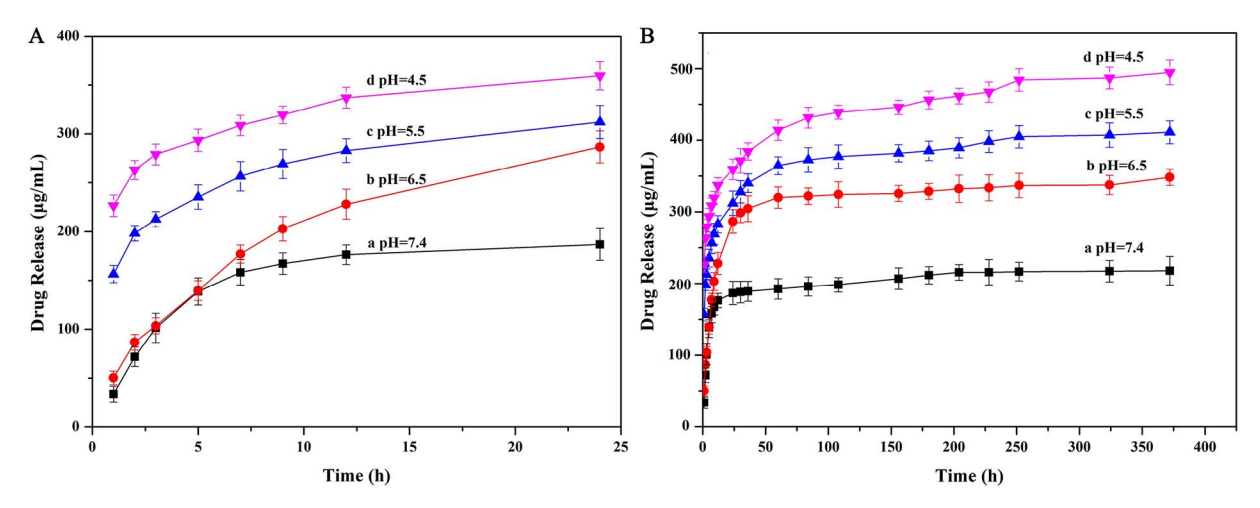
Fig. 3. (A) Digital photographs indicating acid dissolution of ZnO QDs, ZnO-NH₂ and ZnO-FA. Fluorescence spectra of (B) ZnO QDs, (C) ZnO-NH₂, (D) ZnO-FA, incubated at (a) pH = 7.4, (b) pH = 5.5 under an excitation of 340 nm.

pristine ZnO QDs under acidic environment, making sure that ZnO QDs would not dissolve too quickly when the environmental pH changes. All the results prove that the pH-sensitive ZnO-FA with fluorescence has been synthesized successfully.

3.4. Drug release behaviors

Fig. 4A and Fig. 4B show the drug release profiles of ZnO-FA capped TNTs loaded with Van in PBS solution of different pH (7.4, 6.5, 5.5 and 4.5). In the earlier stage, all curves show the same trend of release, i.e., burst release. The difference is the release duration and concentration.

Under neutral condition, the burst release ends quickly within 12 h, and subsequently it almost reaches to a constant concentration of about $195\,\mu\text{g/mL}$. In contrast, the duration of burst release is about 48 h under acidic conditions. After that, it becomes slowly and finally tends to be a stable concentration. Obviously, the equilibrium concentration is decreased with the increase of pH values. In the solution of pH = 4.5 and pH = 5.5, the release of Van is still increased gradually after 16 days. While in the solution of pH = 7.4 and pH = 6.5, the release of Van is tiny after 48 h, and it almost has no change after 6 days, which is due to the fact that ZnO-FA on the surface of TNTs could be dissolved under acidic environments, i.e., they are stable at pH 7.4 but rapidly



 $\textbf{Fig. 4.} \ \ \textbf{The release profile of Vancomycin from TNTs-Van@ZnO-FA system in different buffer.}$

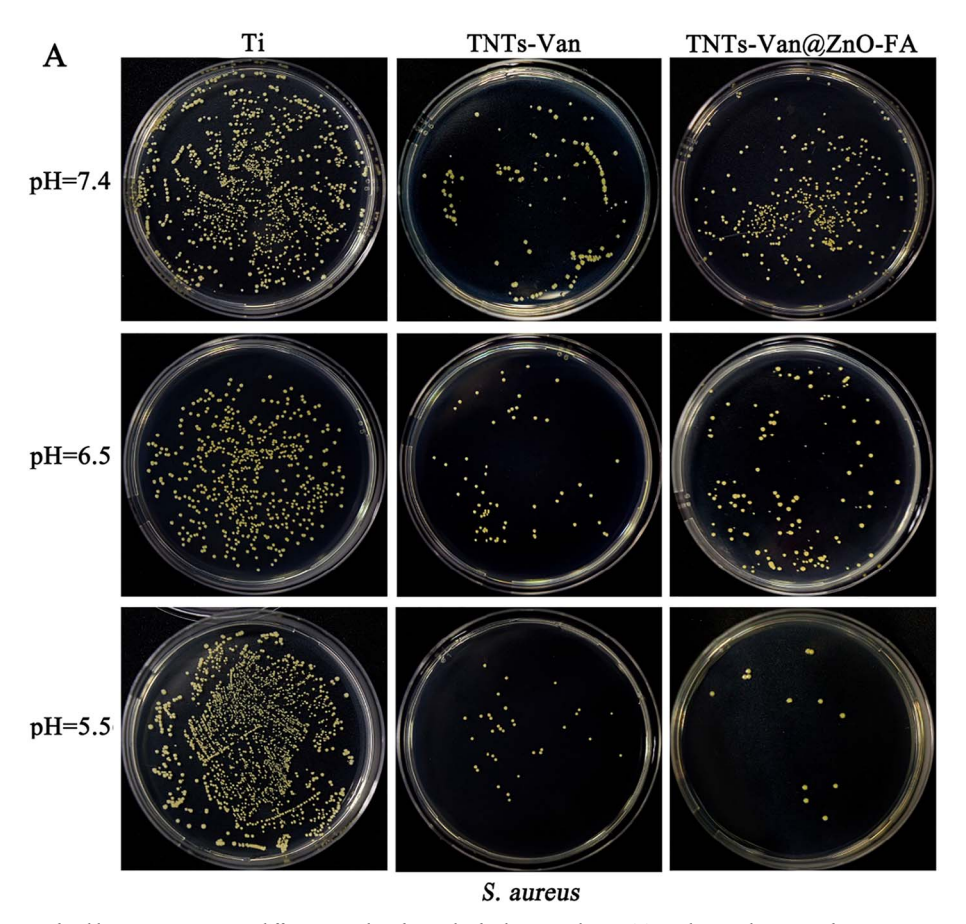


Fig. 5. (A) Representative images of viable *S. aureus* grown on different samples after 24 h of culture are shown, (B) Antibacterial activity of TNTs-Van@ZnO-FA in different pH against *S. aureus* via agar plating method, *p < 0.05, **p < 0.01, ***p < 0.001, n = 3, (C) SEM morphology of *S. aureus* seeded on various samples after incubation at 37 °C for 24 h.

dissolve at pH $\,<\,$ 5.5), then the drugs loaded in TNTs can be released smoothly.

3.5. Antibacterial activity

The antibacterial activities of TNTs-Van@ZnO-FA were analyzed via the spread plate method (Fig. 5A), and the number of viable bacterial colony forming units (CFU) is counted to evaluate the antibacterial ratio (Fig. 5B). As shown in Fig. 5A, when the pH changes from 7.4 to 5.5, the number of bacterial CFU has no visible difference for the control group (Ti), indicating that the pH variation between 5.5 and 7.4 almost has no effects on the growth of bacteria on Ti. In the case of TNTs-Van group, it exhibits far less bacteria than Ti group due to the burst release of Van in an unimpeded way. Furthermore, the number of bacterial CFU is decreased slightly as the pH value decreases. It has been reported that most drugs are almost released rapidly from bare TNTs in the earlier stage [17], thus this group can exhibit higher antibacterial efficacy regardless of the pH variation. Slight decrease of bacteria number at lower pH value is ascribed to rapid release of the remaining drugs with the decrease of pH value. As for TNTs-Van@ZnO-FA group, it exhibits more bacteria than TNTs-Van group under neutral condition because ZnO-FA as a gatekeeper can block the release of drugs. As the pH decreases, bacterial number is significantly decreased, which is caused by the increasing release of drugs with the gradual dissolution of ZnO QDs under acidic conditions. More acidic environment will lead to more rapid dissolution of ZnO QDs, resulting in the release of more drugs from TNTs. This is why when pH is decreased to 5.5, the bacterial CFU number is further decreased significantly.

As shown in Fig. 5B, under neutral condition, the calculated anti-bacterial efficacy of TNTs-Van group and TNTs-Van@ZnO-FA against *S. aureus* is about 85.2% and 60.8%, indicating the ZnO-FA gatekeeper has

obvious effects to prevent the burst release under neutral conditions. Comparing the antibacterial ratios of TNTs-Van groups with different pH, there is a slight increase which could be attributed to the fact that Van inhibits the synthesis of the cell wall structure of S. aureus and the pH would not affect Van's effect [43]. On the contrary, the TNTs-Van@ ZnO-FA groups have a significant increasing antibacterial ratio (from 60.8% to 98.8%) with the pH decreasing, i.e., the antibacterial ratio has been improved over 38% due to the dissolution of ZnO-FA gatekeeper under acidic environments and the drugs change to a quick release. These results are consistent with the results shown in Fig. 5A. In addition, an interesting phenomenon can be found in Fig. 5A and Fig. 5B, i.e., the antibacterial effect of TNTs-Van@ZnO-FA (98.8%) looks a little better than the TNTs-Van (95.1%) at pH 5.5, which could be attributed to the acid dissolution of ZnO QDs into Zn^{2+} (*p < 0.05, **p < 0.01, ***p < 0.001, n = 3). Zinc ions are demonstrated to inhibit multiple activities of bacteria [54]. It has been reported that Zn²⁺ released from ZnO can change the fluidity of the membrane by combining with cell membranes of bacteria, and that ZnO exhibits good antibacterial effect due to a significant enhancement of the oxidative stress [55,56]. As a result, the synergistic action of both Van and zinc ions leads to the destruction of the membrane integrity together, thus inducing better antibacterial effect. The dissolving progress of ZnO is shown in Scheme 2.

To further investigate the morphology and membrane integrity of bacteria, SEM images were taken from the different substrates after incubation (Fig. 5C). The typical morphology was a spherical shape, and the surface was smooth on the control group (Ti). The same intact morphology was observed on the TNTs-Van@ZnO-FA group at neutral conditions, indicating that the ZnO-FA gatekeeper was dissolved little and few drugs were released under neutral conditions. However, *S. aureus* show shape change on the surface of TNTs-Van groups, i.e.,

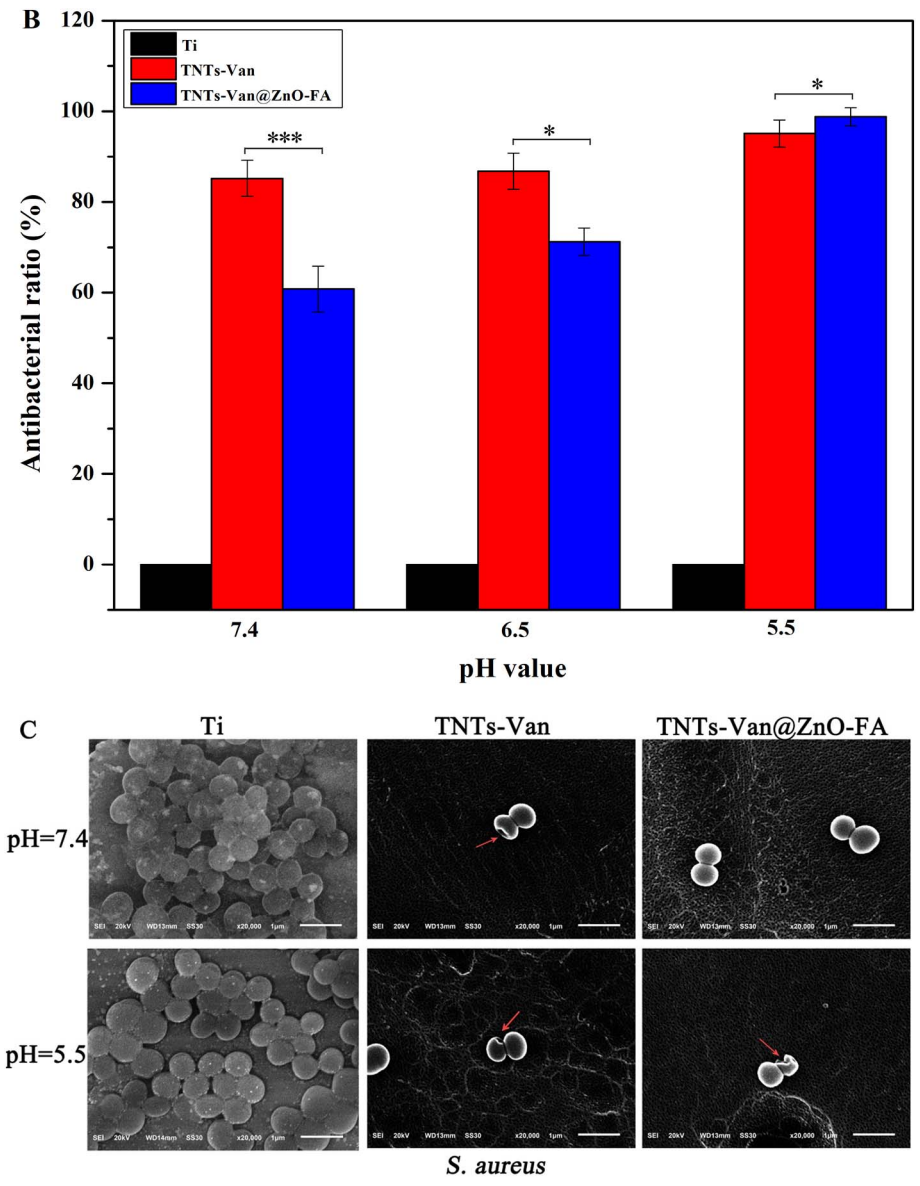


Fig. 5. (continued)

membrane disruption is observed which are due to the fact that Van inhibits the synthesis of the cell wall structure of *S. aureus*. In addition, compared to TNTs-Van groups, a severe membrane corrugation and distorted shapes can be observed on the surface of TNTs-Van@ZnO-FA group under an acidic environment, confirming the better antibacterial effect of TNTs-Van@ZnO-FA group under acidic environment than TNTs-Van groups (98.8% to 95.1% in Fig. 5B).

3.6. Cytotoxicity evaluation

The evaluation of cell proliferation on the samples measured by MTT is shown in Fig. 6. At the early stage (1 day), no significant inhibition of cell proliferation is observed on all the samples. For TNTs samples, an enhanced cell proliferation can be observed as the culture time increases, resulting from the nanostructure of TNTs is conductive to cell proliferation. In the case of TNTs-Van groups, a lower cell viability (86%) can be found compared with the control group (pure titanium), this phenomenon indicates the Van is slightly toxic if overdosed (*p < 0.05, **p < 0.01, ***p < 0.001, versus untreated control (Ti), n = 3) [17]. In addition, during the 1-day to 7-day

incubation periods, the TNTs-Van@ZnO-FA groups show increasing cell toxicity when compared with other groups, which can be attributed to the gradual dissolution of ZnO-FA gatekeeper throughout the incubation periods in vitro, i.e., besides the cytotoxicity of Van with increasing leaching rate, the ZnO exhibits cytotoxicity after dissolution into free Zn 2 + inside cells [57,58].

To investigate the mitosis phase cells, fluorescence morphology was observed through F-actin/nuclei cell staining after culturing for 24 h. The results were observed by IFM and are shown in Fig. 7A. The cells on all samples displays a polygonal and spreading morphology, the antennas of osteoblasts stretch well, and the number of nucleus changes little, suggesting the good biocompatibility of all samples at early stage (24 h). To further understand the impact of structures on osteoblasts, SEM is utilized to observe the surface of cells incubated on samples (Fig. 7B). The cells spread completely into a spindle shape on Ti and TNTs with long threadlike cytoplasmic anchored to the surfaces. Similarly, the cell bodies with well-developed pseudopods can be observed on TNTs-Van and TNTs-Van@ZnO-FA groups after 24 h of culture. These results are in good agreement with the 1-day MTT results shown in Fig. 6.

Scheme 2. The dissolving progress of ZnO.

4. Conclusion

In summary, we have fabricated a drug loading platform using a pH-sensitive ZnO-FA sealed TNTs system, in which the TNTs acted as the loading platform and encapsulated antibacterial drugs of Van. This system can keep stable at physiological pH because of the protection of ZnO-FA on the surface of TNTs. ZnO-FA can be dissolved under the acidic environments, thus Van can be released. Furthermore, when the

pH changes, the ZnO can be degraded into Zn²⁺ completely in the acidic environments and also show antibacterial activity. Thus the antibacterial activity can be significantly enhanced by the combination of Van with ZnO QDs. These advantages make ZnO QDs based pH-responsive system a desirable unique drug loading system for biomedical application including bacterial induced infection.

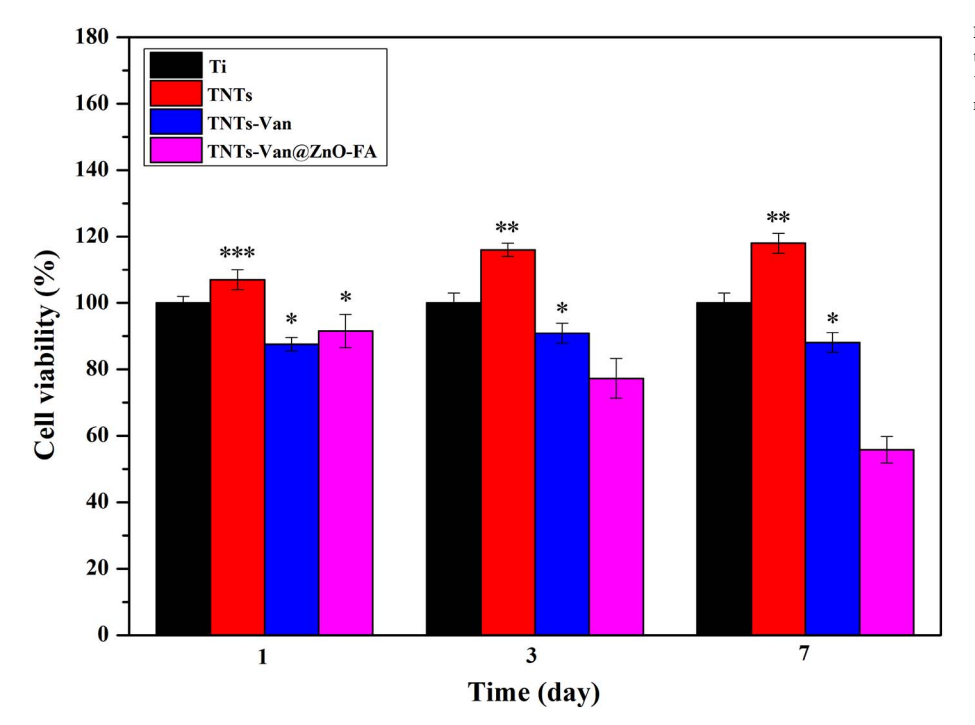


Fig. 6. Cytotoxicity assay of MC3T3-E1 cells viability cultured on different samples for 1, 3, and 7 days, *p < 0.05, **p < 0.01, ***p < 0.001, versus untreated control (Ti), n = 3.

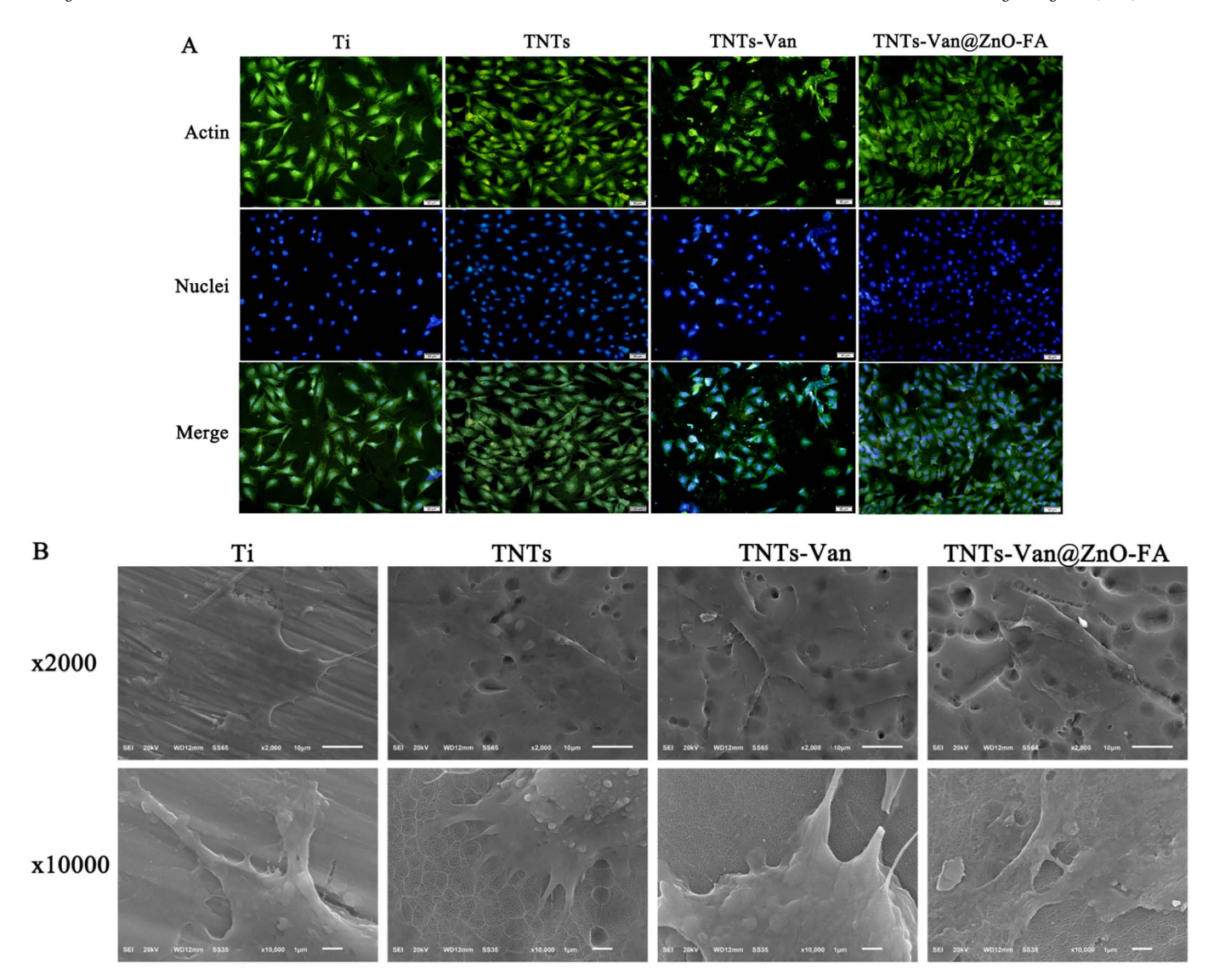


Fig. 7. (A) Fluorescent images of MC3T3-E1 cell cultured on various surfaces for 1 day with actin stained with FITC (green) and nuclei stained with DAPI (blue), (B) SEM morphology of MC3T3-E1 cultured on various surfaces for 1 day with different pH: (a) Ti, (b) TNTs, (c) TNTs-Van, (d) TNTs-Van@ZnO-FA. (For interpretation of the references to color in this figure legend, the reader is referred to the web version of this article.)

Acknowledgements

This work is jointly supported by the National Natural Science Foundation of China, Nos. 51422102, and 51671081, and the National Key Research and Development Program of China No. 2016YFC1100600 (sub-project 2016YFC1100604).

Appendix A. Supplementary data

Supplementary data to this article can be found online at https://doi.org/10.1016/j.msec.2017.12.034.

References

- [1] M. Geetha, A.K. Singh, R. Asokamani, A.K. Gogia, Ti based biomaterials, the ultimate choice for orthopaedic implants a review, Prog. Mater. Sci. 54 (2009)
- [2] S. Wu, X. Liu, K.W.K. Yeung, C. Liu, X. Yang, Biomimetic porous scaffolds for bone tissue engineering, Mater. Sci. Eng. R 80 (2014) 1–36.
- [3] S. Kuroshima, T. Nakano, T. Ishimoto, M. Sasaki, M. Inoue, M. Yasutake, T. Sawase, Optimally oriented grooves on dental implants improve bone quality around implants under repetitive mechanical loading, Acta Biomater. 48 (2017) 433–444.
- [4] E.M. Hetrick, M.H. Schoenfisch, Reducing implant-related infections: active release strategies, Chem. Soc. Rev. 35 (2006) 780–789.

- [5] G. Vermet, S. Degoutin, F. Chai, M. Maton, C. Flores, C. Neut, P.E. Danjou, B. Martel, N. Blanchemain, Cyclodextrin modified PLLA parietal reinforcement implant with prolonged antibacterial activity, Acta Biomater. 53 (2017) 222–232.
- [6] X.Z. Xie, C.Y. Mao, X.M. Liu, Y.Z. Zhang, Z.D. Cui, X.J. Yang, K.W.K. Yeung, H.B. Pan, P.K. Chu, S.L. Wu, Synergistic bacteria killing through photodynamic and physical actions of graphene oxide/Ag/collagen coating, ACS Appl. Mater. Interfaces 9 (2017) 26417–26428.
- [7] K.G. Neoh, X. Hu, D. Zheng, E.T. Kang, Balancing osteoblast functions and bacterial adhesion on functionalized titanium surfaces, Biomaterials 33 (2012) 2813–2822.
- [8] S. Wu, X. Liu, A. Yeung, K.W. Yeung, R.Y. Kao, G. Wu, T. Hu, Z. Xu, P.K. Chu, Plasma-modified biomaterials for self-antimicrobial applications, ACS Appl. Mater. Interfaces 3 (2011) 2851–2860.
- [9] P. Wu, D.W. Grainger, Drug/device combinations for local drug therapies and infection prophylaxis, Biomaterials 27 (2006) 2450–2467.
- [10] T.M. Allen, P.R. Cullis, Drug delivery systems: entering the mainstream, Science 303 (2004) 1818–1822.
- [11] H.Z. Lai, W.Y. Chen, C.Y. Wu, Y.C. Chen, Potent antibacterial nanoparticles for pathogenic bacteria, ACS Appl. Mater. Interfaces 7 (2015) 2046–2054.
- [12] B. Casciaro, M. Moros, S. Rivera-Fernandez, A. Bellelli, J.M. de la Fuente, M.L. Mangoni, Gold-nanoparticles coated with the antimicrobial peptide esculentin-1a(1-21)NH₂ as a reliable strategy for antipseudomonal drugs, Acta Biomater. 47 (2017) 170–181.
- [13] J. Wang, J. Li, S. Qian, G. Guo, Q. Wang, J. Tang, H. Shen, X. Liu, X. Zhang, P.K. Chu, Antibacterial surface design of titanium-based biomaterials for enhanced bacteria-killing and cell-assisting functions against periprosthetic joint infection, ACS Appl. Mater. Interfaces 8 (2016) 11162–11178.
- [14] T. Wang, Z. Weng, X. Liu, K.W.K. Yeung, H. Pan, S. Wu, Controlled release and biocompatibility of polymer/titania nanotube array system on titanium implants,

- Bioact. Mater. 2 (2017) 44-50.
- [15] M. Jin, X. Lu, Y. Qiao, L.N. Wang, A.A. Volinsky, Fabrication and characterization of anodic oxide nanotubes on TiNb alloys, Rare Metals 35 (2016) 140–148.
- [16] K. Zhang, Y. Zhu, X. Liu, Z. Cui, K.W.K. XianjinYang, H. Yeung, S. Wu Pan, Sr/ZnO doped titania nanotube array: an effective surface system with excellent osteoinductivity and self-antibacterial activity, Mater. Des. 130 (2017) 403–412.
- [17] T. Wang, X. Liu, Y. Zhu, Z.D. Cui, X.J. Yang, H. Pan, K.W.K. Yeung, S. Wu, Metal ion coordination polymer-capped pH-triggered drug release system on titania nanotubes for enhancing self-antibacterial capability of Ti implants, ACS Biomater. Sci. Eng. 3 (2017) 816–825.
- [18] C. Xie, P. Li, Y. Liu, F. Luo, X. Xiao, Preparation of TiO2 nanotubes/mesoporous calcium silicate composites with controllable drug release, Mater. Sci. Eng. C 67 (2016) 433–439.
- [19] C.C. Torres, C.H. Campos, C. Diaz, V.A. Jimenez, F. Vidal, L. Guzman, J.B. Alderete, PAMAM-grafted TiO2 nanotubes as novel versatile materials for drug delivery applications, Mater. Sci. Eng. C 65 (2016) 164–171.
- [20] M. Lai, Z. Jin, X. Yang, H. Wang, K. Xu, The controlled release of simvastatin from TiO₂ nanotubes to promote osteoblast differentiation and inhibit osteoclast resorption, Appl. Surf. Sci. 396 (2017) 1741–1751.
- [21] Y. Zhang, L. Chen, C. Liu, X. Feng, L. Wei, L. Shao, Self-assembly chitosan/gelatin composite coating on icariin-modified TiO₂ nanotubes for the regulation of osteoblast bioactivity, Mater. Des. 92 (2016) 471–479.
- [22] J. Xu, X. Zhou, Z. Gao, Y.Y. Song, P. Schmuki, Visible-light-triggered drug release from TiO2 nanotube arrays: a controllable antibacterial platform, Angew. Chem. Int. Ed. 55 (2016) 593–597.
- [23] W. Zhao, J.S. Wei, P. Zhang, J. Chen, J.L. Kong, L.H. Sun, H.M. Xiong, H. Mohwald, Self-assembled ZnO nanoparticle capsules for carrying and delivering isotretinoin to cancer cells, ACS Appl. Mater. Interfaces 9 (2017) 18474–18481.
- [24] Z. Yan, A. Zhao, X. Liu, J. Ren, X. Qu, A pH-switched mesoporous nanoreactor for synergetic therapy, Nano Res. 10 (2016) 1651–1661.
- [25] B.S. Moonga, D.W. Dempster, Zinc is a potent inhibitor of osteoclastic bone resorption in vitro, J. Bone Miner. Res. 10 (1995) 453–457.
- [26] S.L. Hall, H.P. Dimai, J.R. Farley, Effects of zinc on human skeletal alkaline phosphatase activity in vitro, Calcif. Tissue Int. 64 (1999) 163–172.
- [27] H. Hu, W. Zhang, Y. Qiao, X. Jiang, X. Liu, C. Ding, Antibacterial activity and increased bone marrow stem cell functions of Zn-incorporated TiO₂ coatings on titanium, Acta Biomater. 8 (2012) 904–915.
- [28] Y. Yu, G. Jin, Y. Xue, D. Wang, X. Liu, J. Sun, Multifunctions of dual Zn/Mg ion coimplanted titanium on osteogenesis, angiogenesis and bacteria inhibition for dental implants. Acta Biomater. 49 (2017) 590–603.
- [29] B. Wang, Y. Zhang, Z. Mao, D. Yu, C. Gao, Toxicity of ZnO nanoparticles to macrophages due to cell uptake and intracellular release of zinc ions, J. Nanosci. Nanotechnol. 14 (2014) 5688–5696.
- [30] P.E. Petrochenko, Q. Zhang, R. Bayati, S.A. Skoog, K.S. Phillips, G. Kumar, R.J. Narayan, P.L. Goering, Cytotoxic evaluation of nanostructured zinc oxide (ZnO) thin films and leachates, Toxicol. in Vitro 28 (2014) 1144–1152.
- [31] J. Zhang, D. Wu, M.F. Li, J. Feng, Multifunctional mesoporous silica nanoparticles based on charge-reversal plug-gate nanovalves and acid-decomposable ZnO quantum dots for intracellular drug delivery, ACS Appl. Mater. Interfaces 7 (2015) 26666–26673.
- [32] F. Muhammad, M. Guo, W. Qi, F. Sun, A. Wang, Y. Guo, G. Zhu, pH-Triggered controlled drug release from mesoporous silica nanoparticles via intracelluar dissolution of ZnO nanolids, J. Am. Chem. Soc. 133 (2011) 8778–8781.
- [33] X. Zhang, Y. Wang, Y. Zhao, L. Sun, pH-responsive drug release and real-time fluorescence detection of porous silica nanoparticles, Mater. Sci. Eng. C 77 (2017) 19–26.
- [34] D.X. Ye, Y.Y. Ma, W. Zhao, H.M. Cao, J.L. Kong, H.M. Xiong, H. Mohwald, Zno-based nanoplatforms for labeling and treatment of mouse tumors without detectable toxic side effects, ACS Nano 10 (2016) 4294–4300.
- [35] F. Muhammad, M. Guo, Y. Guo, W. Qi, F. Qu, F. Sun, H. Zhao, G. Zhu, Acid de-gradable ZnO quantum dots as a platform for targeted delivery of an anticancer drug, J. Mater. Chem. 21 (2011) 13406.
- [36] N. Tripathy, R. Ahmad, H.A. Ko, G. Khang, Y.B. Hahn, Enhanced anticancer potency using an acid-responsive ZnO-incorporated liposomal drug-delivery system, Nano 7 (2015) 4088–4096.
- [37] Y. Zhang, H. Wang, H. Jiang, X. Wang, Water induced protonation of amine-terminated micelles for direct syntheses of ZnO quantum dots and their cytotoxicity towards cancer, Nano 4 (2012) 3530–3535.

- [38] S.H. Chiu, G. Gedda, W.M. Girma, J.K. Chen, Y.C. Ling, A.V. Ghule, K.L. Ou, J.Y. Chang, Rapid fabrication of carbon quantum dots as multifunctional nanovehicles for dual-modal targeted imaging and chemotherapy, Acta Biomater. 46 (2016) 151–164.
- [39] Y. Song, J. Gao, X. Xu, H. Zhao, R. Xue, J. Zhou, W. Hong, H. Qiu, Fabrication of thermal sensitive folic acid based supramolecular hybrid gels for injectable drug release gels, Mater. Sci. Eng. C 75 (2017) 706–713.
- [40] P. Salari, M. Abdollahi, R. Heshmat, H.A. Mebodi, F. Razi, Effect of folic acid on bone metabolism: a randomized double blind clinical trial in postmenopausal osteoporotic women, Daru 22 (2014) 1–7.
- [41] A.W. Enneman, K.M. Swart, J.P. van Wijngaarden, S.C. van Dijk, A.C. Ham, E.M. Brouwer-Brolsma, N.L. van der Zwaluw, R.A. Dhonukshe-Rutten, T.J. van der Cammen, L.C. de Groot, J. van Meurs, P. Lips, A.G. Uitterlinden, M.C. Zillikens, N.M. van Schoor, N. van der Velde, Effect of vitamin B12 and folic acid supplementation on bone mineral density and quantitative ultrasound parameters in older people with an elevated plasma homocysteine level: B-PROOF, a randomized controlled trial, Calcif. Tissue Int. 96 (2015) 401–409.
- [42] K.A. Rawat, R.K. Singhal, S.K. Kailasa, One-pot synthesis of silver nanoparticles using folic acid as a reagent for colorimetric and fluorimetric detections of 6-mercaptopurine at nanomolar concentration, Sensors Actuators B Chem. 249 (2017) 30–38.
- [43] S. Lin, X. Liu, L. Tan, Z. Cui, X. Yang, K.W.K. Yeung, H. Pan, S. Wu, Porous iron-carboxylate metal-organic framework: a novel bioplatform with sustained anti-bacterial efficacy and nontoxicity, ACS Appl. Mater. Interfaces 9 (2017) 19248–19257.
- [44] M. Li, X. Liu, Z. Xu, K.W. Yeung, S. Wu, Dopamine modified organic-inorganic hybrid coating for antimicrobial and osteogenesis, ACS Appl. Mater. Interfaces 8 (2016) 33972–33981.
- [45] R. Khan, M.S. Hassan, L.-W. Jang, J. Hyeon Yun, H.-K. Ahn, M.-S. Khil, I.-H. Lee, Low-temperature synthesis of ZnO quantum dots for photocatalytic degradation of methyl orange dye under UV irradiation, Ceram. Int. 40 (2014) 14827–14831.
- [46] Y. Xiang, J. Li, X. Liu, Z. Cui, X. Yang, K.W.K. Yeung, H. Pan, S. Wu, Construction of poly(lactic-co-glycolic acid)/ZnO nanorods/Ag nanoparticles hybrid coating on Ti implants for enhanced antibacterial activity and biocompatibility, Mater. Sci. Eng. C 79 (2017) 629–637.
- [47] P. Felbier, J. Yang, J. Theis, R.W. Liptak, A. Wagner, A. Lorke, G. Bacher, U. Kortshagen, Highly luminescent ZnO quantum dots made in a nonthermal plasma, Adv. Funct. Mater. 24 (2014) 1988–1993.
- [48] X. Cui, X. Guan, S. Zhong, J. Chen, H. Zhu, Z. Li, F. Xu, P. Chen, H. Wang, Multistimuli responsive smart chitosan-based microcapsules for targeted drug delivery and triggered drug release, Ultrason. Sonochem. 38 (2017) 145–153.
- [49] Q. Yuan, S. Hein, R.D. Misra, New generation of chitosan-encapsulated ZnO quantum dots loaded with drug: synthesis, characterization and in vitro drug delivery response. Acta Biomater. 6 (2010) 2732–2739.
- [50] X. Cai, Y. Luo, W. Zhang, D. Du, Y. Lin, pH-sensitive ZnO quantum dots-doxorubicin nanoparticles for lung cancer targeted drug delivery, ACS Appl. Mater. Interfaces 8 (2016) 22442–22450.
- [51] Y. Liu, K. Li, J. Pan, B. Liu, S.S. Feng, Folic acid conjugated nanoparticles of mixed lipid monolayer shell and biodegradable polymer core for targeted delivery of Docetaxel, Biomaterials 31 (2010) 330–338.
- [52] Y. Zhu, X. Liu, K.W.K. Yeung, P.K. Chu, S. Wu, Biofunctionalization of carbon nanotubes/chitosan hybrids on Ti implants by atom layer deposited ZnO nanostructures. Appl. Surf. Sci. 400 (2017) 14–23.
- [53] S. Mohapatra, S.K. Mallick, T.K. Maiti, S.K. Ghosh, P. Pramanik, Synthesis of highly stable folic acid conjugated magnetite nanoparticles for targeting cancer cells, Nanotechnology 18 (2007) 385102.
- [54] T.N. Phan, T. Buckner, J. Sheng, J.D. Baldeck, R.E. Marquis, Physiologic actions of zinc related to inhibition of acid and alkali production by oral streptococci in suspensions and biofilms, Oral Microbiol. Immunol. 19 (2004) 31–38.
- [55] T.A. Söderberg, B. Sunzel, S. Holm, Antibacterial effect of zinc oxide in vitro, Scand. J. Plast. Reconstr. Surg. 24 (1990) 193–197.
- [56] G. Applerot, A. Lipovsky, R. Dror, N. Perkas, Y. Nitzan, R. Lubart, A. Gefanken, Enhanced antibacterial activity of nanocrystalline ZnO due to increased ROSmediated cell injury, Adv. Funct. Mater. 19 (2010) 842–852.
- [57] X. Deng, Q. Luan, W. Chen, Nanosized zinc oxide particles induce neural stem cell apoptosis, Nanotechnology 20 (2009) 115101.
- [58] K.D. Kroncke, Cellular stress and intracellular zinc dyshomeostasis, Arch. Biochem. Biophys. 463 (2007) 183–187.